



Combustion synthesis of titania nanoparticles in a premixed methane flame

Hsiao-Kang Ma*, Hsiung-An Yang

Department of Mechanical Engineering, National Taiwan University, No. 1, Sec. 4, Roosevelt Road, Taipei 106, Taiwan

ARTICLE INFO

Article history:

Received 17 August 2009

Received in revised form 12 May 2010

Accepted 21 May 2010

Available online 27 May 2010

Keywords:

Combustion synthesis

Titania nanoparticles

Crystal structure

X-ray diffraction

Transmission electron microscope

ABSTRACT

Previous studies have shown that titanium tetra-isopropoxide (TTIP) can be a substitute in the production of non-poisonous and inexpensive nanostructured titania (TiO_2) particles. This study discusses the combustion characteristics of synthesized titania obtained while adding TTIP into the premixed methane/air flames. As the TTIP concentration increased, a bright yellow flame brush, representing a region of titania nanoparticles production, appeared on the tip of the flame's inner luminous cone. The crystal structure of the synthesized nanoparticles was analyzed using X-ray diffraction (XRD) and transmission electron microscope (TEM). The Barrett, Joyner, and Halenda (BJH) model was used to estimate the pore volume and pore size of the titania. Additionally, the specific surface area (SSA) of the synthesized titania nanoparticles was measured by a Brunauer–Emmett–Teller (BET) apparatus (Micromeritics ASAP 2020). The variation of the molar ratio (of oxygen-to-nitrogen) had an important influence on the temperature distribution and, accordingly, on the particle kinetics. It was found that in the flame temperature range from 1138 to 1290 K, the anatase content of the titania particles increased in direct proportion with the oxygen concentration. Moreover, high-purity anatase titania nanoparticles that were 20 nm in diameter were synthesized in methane/air flames with a TTIP concentration of about 0.26%. Overall, as the TTIP concentration increased, the flame temperature decreased, and it yielded a slightly higher percentage of rutile titania nanoparticles. The best titania macroporous–mesoporous structure was more preferable than the commercial Degussa P25 titania in terms of a higher percentage of anatase nanoparticles, a smaller mean particle diameter (Z -average), a higher BET SSA, and a larger pore volume and pore size. The photocatalytic properties of the flame-synthesized titania nanoparticles and commercial Degussa P25 were compared regarding the degradation of methyl orange. In the results, the flame-synthesized titania nanoparticles ($\phi = 1.0$, TTIP = 0.32%, $\text{O}_2/\text{N}_2 = 40/60$) were more efficient in the removal of methyl orange.

© 2010 Elsevier B.V. All rights reserved.

1. Introduction

Previously, commercial titania particles (Degussa P25) have been synthesized from the hydrolysis of toxic vapor (TiCl_4) in an oxy-hydrogen flame via the so-called “chloride process” [1]. According to the literature, the formation of flame-synthesized titania particles from the TiCl_4 precursor has been studied extensively [2]. Nevertheless, the metal-organic compound titanium tetra-isopropoxide (TTIP) is more favorable than the commonly used dopant TiCl_4 because it can be used in a chlorine-free flame without any corrosive hazards. Thus, TTIP can be used as a substitute precursor in the synthesis of titania particles. Moreover, this precursor is capable of creating microspherical titania particles, which could have many interesting applications [3].

In 2006, Akurati et al. [4] found loose spherical agglomerates of small-size particles (90 nm) and a rutile content with up to 35 wt.%

at low oxygen-flow rates, whereas large anatase-rich aggregates were found at high oxygen-flow rates. Further, the amount of rutile content is reported to increase with the dilution of TTIP precursor by oxygen. Using the sol–gel method at various sintering temperatures, Setiawati and Kawano [5] found significant suppression of the titania particle growth and stabilization of the anatase phase after doping rare-earth (RE) Eu and Sm ions into titania nanoparticles prepared from 673 to 1223 K for 1 h. Using a diffusion flame, Chang et al. [6] successfully obtained 13-nm crystalline titania nanoparticles from a TTIP precursor. Moreover, a high flame temperature and low precursor concentration were shown to enhance the evaporation of liquid droplets, and the evaporated precursors underwent a vapor phase reaction, resulting in aggregates consisting of small nanoparticles. Chen et al. [7] discovered that the well-aligned RuO_2 nanorods (NRs) could be grown on top of the tips of rutile phase titania NRs deposited on a sapphire (1 0 0) substrate via metal-organic chemical vapor deposition (MOCVD) using TTIP as a source reagent. Periyat et al. [8] achieved the formation of 100% anatase at 1123 K and 41% anatase at 1173 K, and their modification using $(\text{NH}_4)_2\text{SO}_4$ was found to significantly increase

* Corresponding author. Tel.: +886 2 23629976; fax: +886 2 23632644.

E-mail addresses: skma@ntu.edu.tw, an0307@hotmail.com (H.-K. Ma).

the surface area of the titania. Currently, the synthesis of mesoporous titania microspheres of fairly high surface area ($219 \text{ m}^2/\text{g}$) with uniform 6–7 nm wide wormlike channels using a spray pyrolysis technique with a block copolymer templating approach has been demonstrated by Beitollahi et al. [3]. Recently, nanocrystalline titania powders have been synthesized by direct calcination of the Ti-base-coupling agent [9].

Titania nanoparticles have long been of considerable research interest for their chemical energy conversion and ideal environmental photocatalyst properties; more specifically, these nanoparticles are non-toxic, stable, abundant and inexpensive [10]. The growth behavior of the titania nanoparticles has a significant influence on the crystallinity and surface area, and this behavior can be controlled by different process parameters [11]. In general, the size and shape of the nanoparticles are important for industrial applications, such as ease of milling and high opacity of the powder [12]. The photocatalytic efficiency of anatase titania has proven to be better than rutile titania, which is thus more favorable for filtering polluted air and wastewater [13]. Additionally, the ability to control characteristics of the functional nanoparticles or nanotubes through flame synthesis would improve the final product and save energy [14]. In real-life applications, titania nanoparticles are not only widely employed as white pigments, photocatalysts and semiconductors but are also applied in dye-sensitized solar cells [15,16]. Therefore, the combustion synthesis method has become a common one-step synthesis of titania nanoparticles. This method is an interesting research area because it is able to mass-produce; it is cleaner and more energy-efficient; it is a continuous process with minimal post-treatment; and it is easier to employ than the traditional wet-chemical and chemical vapor deposition methods [17].

Our previous studies [18] investigated the influence of the flame condition, TTIP concentration, and hexamethyldisiloxane (HMDS) on the crystal phase purity and particle morphology of titania synthesized in TTIP/HMDS flames. It was found that for Si to Ti atomic ratios of over 0.375, the agglomerates of SiO_2 particles become dominant and there is almost no formation of titania crystals. Nonetheless, the details of the phase composition and morphology of synthesized titania particles associated with TTIP oxidation in flames are not well characterized. In this study, an experimental investigation of the synthesis of titania particles through TTIP oxidation was conducted in premixed methane/air flames to study the influences of flame temperature, precursor concentration, oxygen molar fraction, and particle collecting height on the crystalline phase and particle morphology of titania nanoparticles. The specific surface area (SSA) of the synthesized titania nanoparticles was measured via a Brunauer–Emmett–Teller (BET) apparatus. Additionally, the photocatalytic properties of the flame-synthesized titania nanoparticles and commercial Degussa P25 were compared regarding the degradation of methyl orange.

2. Experimental details

2.1. Experimental setup

Titania nanoparticles were synthesized in premixed flames by using titanium tetra-isopropoxide $\text{C}_{12}\text{H}_{28}\text{TiO}_4$ (TTIP, 97% purity, Acros Organics) as the titania precursor. TTIP liquid was contained in a flask, which was connected with gas-carrying lines. TTIP vapor was then carried by bubbling air through the liquid, as shown in Fig. 1. In this experiment, the feeding rates for all of the injections are given in Table 1.

The premixed flame burner used in this study was composed of two parts. The bottom portion was in a divergent shape to decrease the flow velocity, and it was filled with small steel balls to encourage the mixing of methane and air. The upper portion was a stainless steel tube with a diameter of 12 mm near the exit port of the burner, and several layers of steel wire screen were installed to ensure the uniformity of gas flow. Premixed gases were prepared by air with methane or hydrogen, which were blended in a mixing chamber filled with small glass balls. Before entering the burner, the combustible mixture was further mixed with TTIP vapor that was carried by an air-stream in the other mixing chamber, which was also filled with

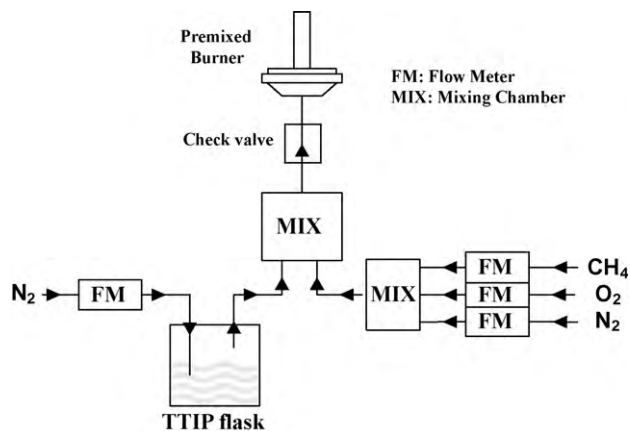


Fig. 1. Experimental setup for combustion synthesis of titania particles.

glass balls. The synthesized titania nanoparticles in the post-flame region were collected via deposition on a stainless steel plate, which was inserted into the flame zone at different heights (h) above the burner exit port.

A high-resolution digital camera (Sony DSC-F717) was applied to acquire flame images; thus, we investigated the flame structures under different equivalence ratios and TTIP concentrations. Flame temperatures were measured using $125\text{-}\mu\text{m}$ Pt/Pt-13% Rh thermocouples and were corrected for radiative heat loss [19]. The emissivity (ϵ) of titania-coated Pt/Pt-13% Rh thermocouples was adopted in the radiation concentration procedure. To derive detailed temperature profiles from the flame zone, the thermocouple was positioned on an automatic positioner. The movement of this positioner was controlled by a programmable motor-driven stage with a minimum moveable distance of 0.01 mm in three tangential axes.

2.2. Composition analysis

The size and morphology of synthesized particles were examined under a transmission electron microscope (TEM, Hitachi H-7110) operating at 75 kV. The phase composition of the titania particles was investigated by an X-ray diffraction (XRD) analysis (Philips X'Pert Pro; with $\text{CuK}\alpha$ radiation). The XRD analysis was conducted with as-synthesized particles and heat-treated particles at different temperatures. The weight fractions of anatase and rutile phases in the sample were calculated from the relative intensity of the strongest peaks corresponding to anatase [$2\theta = 25.3^\circ$ for the (1 0 1) reflection of anatase] and rutile [$2\theta = 27.3^\circ$ for the (1 1 0) reflection of rutile] phases, as described by Spurr and Myers [20]. The weight fraction of anatase phase (Y_A) in the titania sample was determined by Eq. (1), where I_A and I_R are the intensities of the strongest XRD peaks for anatase and rutile titania, respectively:

$$Y_A = \frac{1}{1 + 1.26(I_R/I_A)} \quad (1)$$

The Barrett, Joyner, and Halenda (BJH) model was used to estimate the pore volume and pore size of the titania powders according to the nitrogen adsorption isotherms at 77 K. Additionally, the SSA of the synthesized titania nanoparticles collected on a stainless steel plate was measured by a Brunauer–Emmett–Teller (BET) apparatus (Micromeritics ASAP 2020). The average primary particle size (D_p)

Table 1
Feeding rates of all the injections.

O_2/N_2	Methane (L/min)	O_2 (L/min)	N_2 (L/min)	ϕ
20/80	0.15	0.75	3.00	0.8
		0.30	1.20	1.0
		0.50	2.00	1.2
25/75	0.18	0.90	2.70	0.8
		0.36	1.08	1.0
		0.60	1.80	1.2
30/70	0.21	1.05	3.50	0.8
		0.42	0.98	1.0
		0.70	1.63	1.2
35/65	0.24	1.20	2.23	0.8
		0.48	0.89	1.0
		0.80	1.49	1.2
40/60	0.27	1.35	2.03	0.8
		0.54	0.81	1.0
		0.90	1.35	1.2
















Test No.	1	2	3	4	5
TTIP mass flow rate (g/min.)	0	0.013	0.022	0.077	0.123
Concentration (%)	0	0.06	0.1	0.35	0.56
$\phi = 1.0$					
$\phi = 1.2$					
$\phi = 0.8$					

Fig. 2. Recorded images of methane/air flames with different ϕ and TTIP concentration.

was calculated by assuming that all titania particles have the same spherical shape and size. D_p is calculated by Eq. (2), as

$$D_p = \frac{6}{(SSA) \times (\rho)} \quad (2)$$

where SSA is the BET-specific surface area and ρ is the density of anatase titania particles (3.84 g/cm^3). Size measurements were performed using dynamic light scattering (DLS) on a Malvern Zetasizer Nano-ZS at 298 K. Samples were irradiated with red light (HeNe laser, wavelength $\lambda = 632.8 \text{ nm}$), and the intensity fluctuations of scattered light (detected at a back scattering angle of 173°) were analyzed to obtain an autocorrelation function. The mean particle diameter (Z-average) was calculated by the software DTS v6.01 from the particle distributions measured according to the international standard ISO 13321, and the polydispersity indices (Pdl) were given as a measure of the size ranges present in the solution.

The photocatalytic activities of the flame-synthesized titania nanoparticles and commercial Degussa P25 were evaluated by the degradation of methyl orange, for which the activity analyses were carried out using a vertical tubular batch reactor made of quartz. The entire reactor was enclosed inside a UV-light house, and the light house was equipped with eight UV-light tubes (maximum intensity at 300 nm), each having a power of 12 W. Then, 0.25 g/L of titania powders was placed into a 200-mL aqueous solution of $4 \times 10^{-5} \text{ M}$ methyl orange [21]. Next, the suspension was magnetically stirred in the dark for 30 min to reach the adsorption equilibrium of methyl orange on the powders prior to irradiation. During irradiation, the suspension was sampled at regular intervals and immediately centrifuged to remove catalyst particles. The photocatalytic degradation was monitored by measuring the absorbance of the solution samples with a UV-vis spectrophotometer (Hitachi U3410). The concentration of organic dye was determined by measuring methyl orange under the absorption at $\lambda = 465 \text{ nm}$ under UV-vis spectroscopy.

2.3. Test conditions

Premixed methane/air flames were prepared with the equivalence ratios (ϕ) of 0.8, 1.0, and 1.2. The equivalence ratio was used to describe the premixed methane/air flame, defined as the ratio of the actual fuel-oxidizer ratio to the ratio for a stoichiometric process. Therefore, it was calculated based upon the quantities of fuel (methane) and oxidizer in the reactant mixture. Because the amounts of precursor TTIP introduced into the premixed mixture were very small, they were neglected in the calculation of the equivalence ratio.

Nitrogen gas was used as a diluent in the oxidizer stream. To investigate the influence of the oxygen concentration on the titania synthesis, the oxidizer was prepared to have compositions including four molar ratios of oxygen-to-nitrogen (O_2/N_2), which were 20/80, 30/70, 35/65, and 40/60. The amount of TTIP vapor intro-

duced into the flame zone was calibrated with respect to the carrying-gas flow rate. The concentrations of TTIP in the premixed, combustible mixture were adjusted to have concentrations of 0.32, 0.34, 0.36, 0.38, and 0.40%.

3. Results and discussion

3.1. Observation of methane/air flames with TTIP

The specific concentration % of TTIP is defined as the TTIP molar fraction/(methane mole fraction + oxygen mole fraction + nitrogen mole fraction). In test no. 1, which is shown in Fig. 2, a double flame structure with an internal premixed flame and an external diffusion flame was observed [22]. As a small amount of TTIP (0.06%) was added into the premixed mixtures, a flame secondary from the internal premixed flame, orange in color, was attributed to the black-body radiation from titania particles (for interpretation of the references to color in this sentence, the reader is referred to the web version of the article). When the TTIP concentration increased up to 0.1% and above, the appearance of a bright yellow flame brush was observed, following the tip of the conical luminous zone of the methane/air flames. Also, the inner luminous cone of flames was axially protracted when the bright flame brush became visible. Then, the internal premixed flame could not be observed with $\phi = 1.0$ and a TTIP concentration of 0.56. The flame brush became stronger in radiation intensity and larger in size as the TTIP concentration increased. In the bright flame brush, which may represent a particle-laden region, there were a number of flame-synthesized titania particles. It was found that greater concentrations of titanium precursors yielded higher intensities of the flame brushes. The increasing TTIP concentration would lead to increases in the flame length and rutile titania content. The leaner flames ($\phi = 0.8$) showed low luminosity and appeared pale blue.

With a higher equivalence ratio of $\phi = 1.2$ and a TTIP concentration of 0.06%, a bright flame brush appeared. This could have been

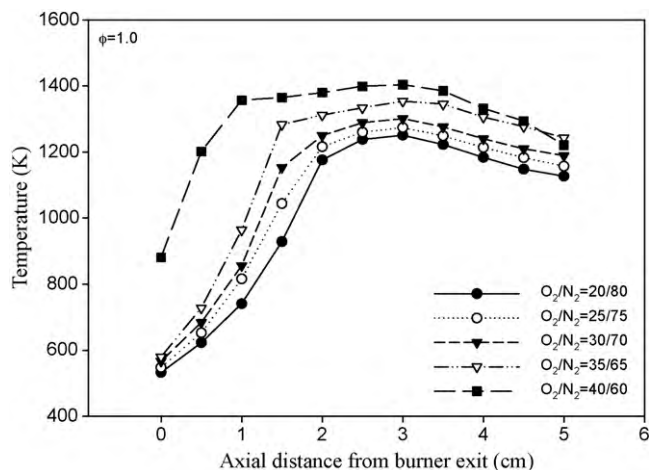


Fig. 3. Axial temperature profiles with different oxygen-to-nitrogen molar ratio ($\phi = 1.0$).

caused by the effect of emission and synthesis kinetics (due to the increase in flame temperature). In contrast, under a flame condition of $\phi = 0.8$, the flame brush was not observed until the TTIP concentration reached 0.56%. When the concentrations of the titanium precursor were from 0 to 0.56%, a secondary orange flame around the inner luminous cone was observed in the flame of $\phi = 1.0$. Therefore, it was apparent that when the equivalence ratio of the flames was larger, the flame brush appeared with a lower TTIP concentration.

3.2. Measured temperature profiles of particle-laden flames

Step axial temperature gradients, usually existing in premixed flames, were contributing factors for the particle size distribution. Also, the growth of the particles was very sensitive to the temperature. In Fig. 3, it is seen that the flame temperature rose as the oxygen molar fraction in the oxidizer increased, due to the reduction of the nitrogen that acted as a diluent in the flame. Moreover, with a higher oxygen ratio in the oxidant, the flame exhibited a faster temperature rise and a more uniform temperature in the post-flame region, until the point about 4 cm away from the flame cone. It is useful to note that the gas temperature at the burner exit was mainly influenced by the temperature of burned gas, due to the heat feedback from the post-flame region. Because no preheating of the reactant mixture was conducted under the condition without TTIP, a variation of the gas temperature between 500 and 900 K was observed at the burner exit.

Fig. 4 shows that the presence of synthesized particles tended to increase the radiative loss from the flame and thus lowered the flame temperature. Gas temperatures at the burner exit varied between 400 and 500 K. This was caused by the fact that premixed mixtures containing TTIP were preheated at 398 K to prevent the TTIP vapor from condensing and by the heat feedback from the post-flame region. The flame temperature increased with the axial distance (z) from the burner exit to $z = 3.5$ cm, which corresponds to the height of the inner luminous cone. Then, the flame temperature remained almost constant with the axial distance up to $z = 5$ cm, beyond which the temperature started to decrease. The axial temperature profiles of the flames with the addition of 0.4% TTIP were lower than those flames with fewer titanium precursors.

3.3. Effect of flame condition on the purity of titania particles

The collected flame-synthesized particles consisted of mostly white powders and a small amount of brown powders. The white

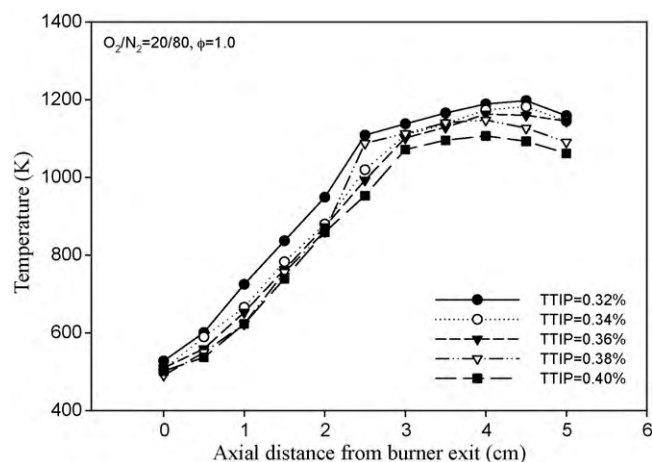


Fig. 4. Axial temperature profiles with different TTIP concentration ($O_2/N_2 = 20/80$, $\phi = 1.0$).

powders were titania particles, and the brown powders could have been titanium monoxide (TiO) or carbon particles. To further confirm the composition, X-ray diffraction (XRD) analysis was conducted with selected particles.

Fig. 5 indicates that the synthesized particles consisted of both anatase and rutile titania. The intensity of the strongest peak for the anatase titania (labeled \circ at $2\theta = 25.3^\circ$) rose with an increase in the oxygen-to-nitrogen molar ratio, implying that the anatase content in the particles increased with the oxygen concentration in the mixture. In contrast, the intensity of the strongest peak for the rutile phase (labeled \bullet at $2\theta = 27.5^\circ$) decreased with an increase in the oxygen-to-nitrogen molar ratio. There was a higher anatase content when the oxygen molar fraction became higher in the reactant mixture, and this is due to the relatively high oxygen availability during the titania particle formation, which is in agreement with Rulison et al. [23]. It is important to note that the increase of the oxygen molar fraction in the oxidizer led to an increase in the flame temperature. The effect of flame temperature on the crystalline phase of titania is presented in Fig. 6.

Based upon the quantitative analysis calculated by Eq. (1), there was a variation of the anatase weight fraction (wt.%) with the oxygen molar fraction in the oxidizer. The results showed a significant increase in the anatase content with the oxygen concentration in the oxidizer. In a flame with $\phi = 1.0$ and a TTIP concentration

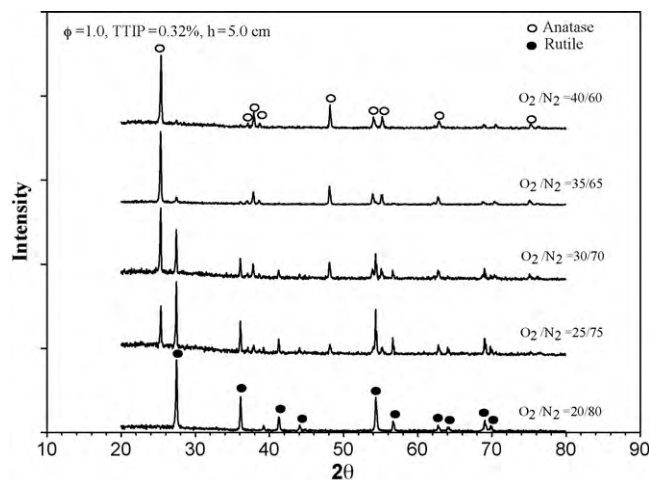


Fig. 5. XRD spectra of synthesized particles with different oxygen-to-nitrogen molar ratio ($\phi = 1.0$, TTIP = 0.32%, $h = 5.0$ cm).

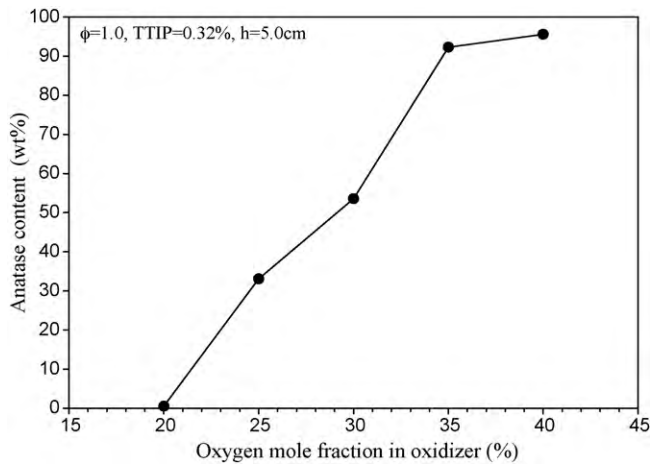


Fig. 6. Effect of oxygen-to-nitrogen molar ratio on anatase content of titania particles ($\phi = 1.0$, TTIP = 0.32%, $h = 5.0$ cm).

of 0.32%, the anatase content of about 0 wt.% at $O_2/N_2 = 20/80$ in the oxidizer stream increased up to 97.7 wt.% at $O_2/N_2 = 40/60$. As indicated by Rulison et al. [23], feeding $TiCl_4$ precursor concentrations into the oxidizer stream yielded mainly anatase titania powders. This was in accordance with the known atmosphere-dependent anatase-to-rutile transformation, which occurred more rapidly as the ambient oxygen concentration decreased. Moreover, our experiment showed that the lack of rutile titania yielded in the flame with high oxygen-to-nitrogen ratios in the oxidant was mainly due to the high ambient oxygen concentration. This finding confirmed the conclusion drawn by the above authors, which led to a low concentration of oxygen vacancies within the crystal. Fig. 7 shows the effect of temperature profiles with different oxygen-to-nitrogen molar ratios on the anatase content of titania particles under the operating conditions at $\phi = 1.0$, TTIP = 0.32%, and $h = 3.0$ cm. Obviously, the higher flame temperature with the sufficient oxygen concentration triggered the crystallization and growth of the anatase phase.

The effect of the particle residence time in the flame on the phase composition of titania particles was further studied by collecting the product at different heights (h) above the burner exit. Fig. 8 presents the anatase content in the product collected at $h = 3.0$ – 5.0 cm. An obvious decrease in the anatase content of the particles with collecting height was observed. This result was consistent with the observation by Vemury and Pratsinis [24], indi-

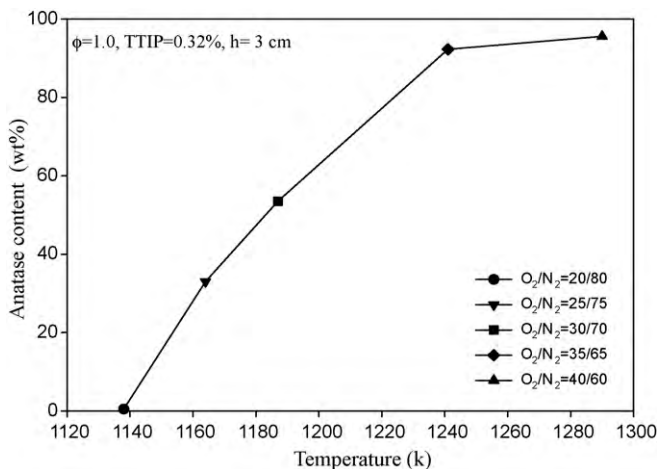


Fig. 7. Effect of temperature profiles with different oxygen to the nitrogen molar ratio on anatase content of titania particles ($\phi = 1.0$, TTIP = 0.32%, $h = 3.0$ cm).

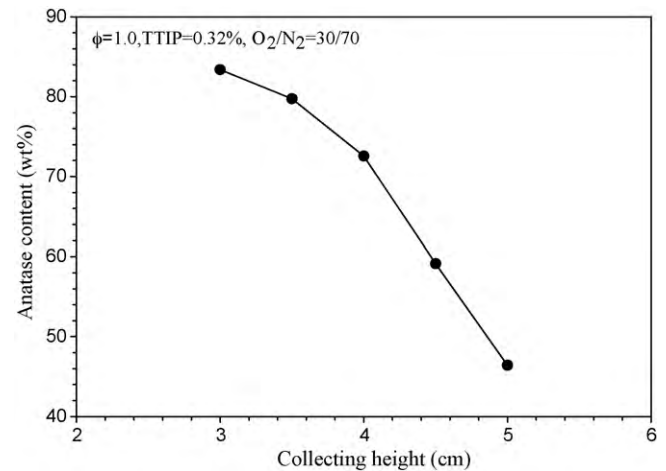


Fig. 8. Effect of collecting height of particles in flame on anatase content of titania particles ($\phi = 1.0$, TTIP = 0.32%, $O_2/N_2 = 30/70$).

cating that the reduction of particle residence time results in a lower level of crystallinity.

In Fig. 9, the anatase content was found to decrease with the increase of the TTIP concentration. This finding was attributed to the change in the flame temperature, which rose with increasing TTIP concentration. Because the transformation of anatase-to-rutile was enhanced by a higher flame temperature, the anatase content was decreased in the flame supplemented with a larger amount of TTIP [25].

According to the previous studies, as the titania particles stayed in the flame, due to collisions, the titania crystalline phase changed from anatase-to-rutile. Moreover, in the experiment, the increase of TTIP density resulted in a longer flame, which caused an increase of the rutile content. Also, high-purity anatase titania particles were synthesized in methane/air flames with a low TTIP concentration of about 0.26% in Fig. 10. The rutile main peak ($2\theta = 27.5^\circ$) strength grew after an increase of density, which was in compliance with the results in the literature.

3.4. Particle formation and specific surface area

Fig. 11 shows that the particle size distribution is quite broad and ranges from 10 to 150 nm and 10 to 200 nm for the particles produced with oxygen-to-nitrogen molar ratios of 20/80 and 40/60,

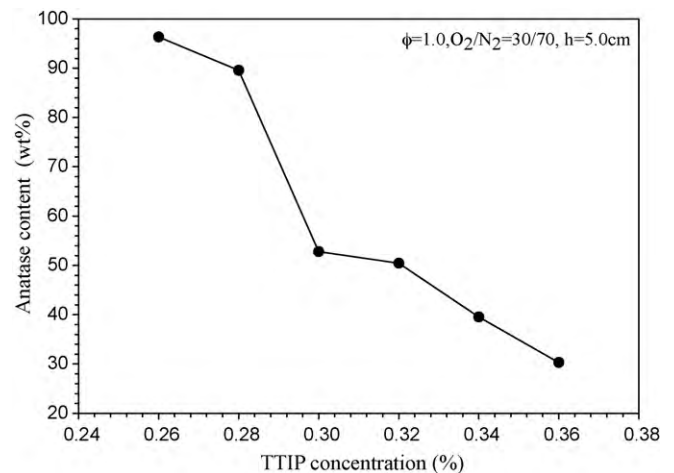


Fig. 9. Effect of TTIP concentration on the anatase content of titania particles ($\phi = 1.0$, $O_2/N_2 = 30/70$, $h = 5.0$ cm).

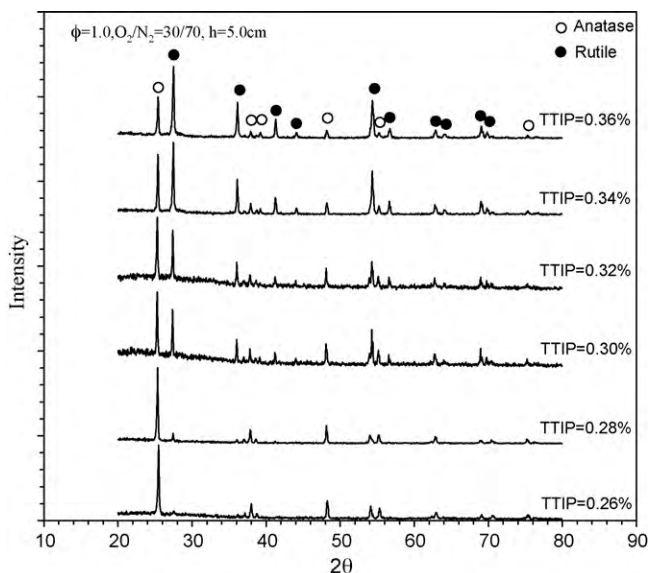


Fig. 10. Effect of TTIP concentrations on anatase/rutile content of titania particles ($\phi = 1.0$, $O_2/N_2 = 30/70$, $h = 5.0$ cm).

respectively. The range of the particle size distribution tended to be wider with increasing oxygen-to-nitrogen molar ratio because of the concomitant increase of flame temperature. Nucleated clusters of titania particles grew by coagulation and coalescence as they traversed through the high-temperature flame. A higher oxygen percentage resulted in a temperature rise that led to bigger particle sizes and the gathering of particles and uneven particle sizes. The anatase phase had a better ability to absorb light compared to darker particles, as shown in Fig. 11(b).

Fig. 12 shows that small particles of about 65 nm were formed and agglomerated into large flocs. As these flocs flowed upward into regions of higher temperature, they compacted to form larger particles, as shown in Fig. 12(b). Subsequent surface growth and aggregation caused the continued evolution of particles. Thus, the nearly spherical titania particles, shown in Fig. 12(a) with diameters of around 10–25 nm, were formed at $h = 3.0$ cm. These variations of particle morphology with increasing residence time and temperature nicely confirmed the evolution of titania particle formation

sketched by Hung and Katz [26]. As far as the crystalline phase was concerned, the nanosize particles (around 20 nm, at 1290 K) collected at $h = 3.0$ cm should have made up a significant fraction of the anatase phase, as the rutile content grew with increases of the residence time in the flame. There was a similar trend of increased broad particle size distribution with a decrease in collecting height, and this associated with the decreased residence time of the particles.

Table 2 shows the pore volume and pore size of titania nanoparticles synthesized at different molar ratios of O_2/N_2 . When the D_p decreased from 13.14 to 12.56 nm, the pore volume increased from 0.278 to 0.297 cm^3/g and the pore size enlarged from 9.35 to 9.55 nm. As the D_p were 13.14 and 12.56 nm, the BET SSA of titania particles were 118.94 and 124.39 m^2/g , respectively. These results suggest that the developed titania particle was a macroporous–mesoporous material and that the measured BET SSA was mostly attributed to the nanosize of the crystallites.

3.5. A comparison of titania nanoparticles

Table 2 compares the pore volume and pore size of titania nanoparticles synthesized at different molar ratios of O_2/N_2 . The pore volume was 0.297 cm^3/g and the pore size was 9.55 nm when the D_p was 12.56 nm. Moreover, the BET SSA of titania particles was 124.39 m^2/g , which was mostly attributed to the small particle size of the crystallites. The results were indeed more preferable than those for the commercial Degussa P25 titania. Table 2 also shows the Z-average and the XRD measurements for the phase composition (weight percentage of anatase and rutile) at different molar ratios of O_2/N_2 . Clearly, the BET SSA increased as the Z-average decreased with the increased molar ratio of O_2/N_2 . This result is consistent with the observations from the TEM image analysis. Obviously, the particles have limited aggregation according to the D_p calculated from the TEM image analysis, but they were larger than the average particle size calculated from the BET SSA. As depicted in Table 2, the highest anatase concentration in the titania particles was made at molar ratios of O_2/N_2 from 20/80 to 40/60, with the TTIP concentration at 0.32%. This is what would be expected: a higher temperature and a larger molar ratio of O_2/N_2 favor the transformation from rutile to anatase crystal phases.

Fig. 13 shows the photocatalytic activity of the flame-synthesized titania nanoparticles in comparison with commercial Degussa P25 regarding the removal of methyl orange as a function

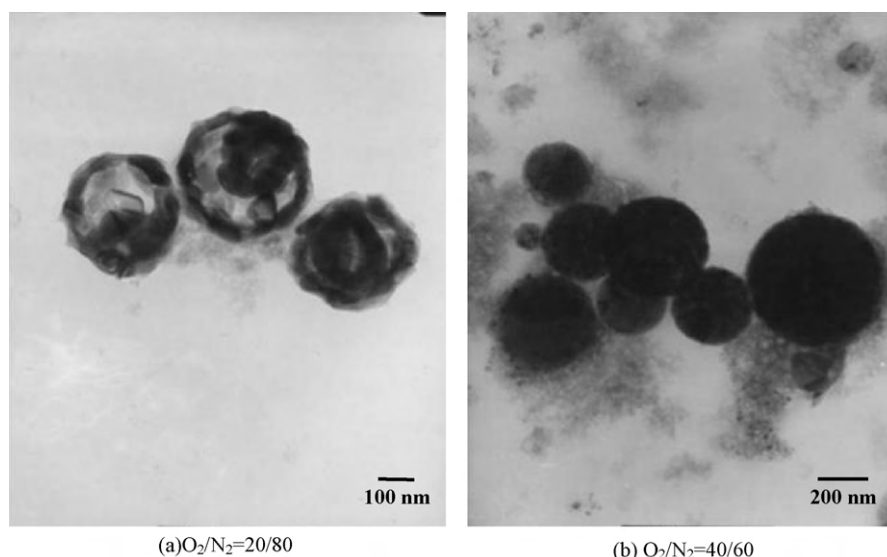


Fig. 11. TEM micrographs of synthesized titania particles collected at (a) $O_2/N_2 = 20/80$ and (b) $O_2/N_2 = 40/60$ ($\phi = 1.0$, TTIP = 0.32%, $h = 5.0$ cm).

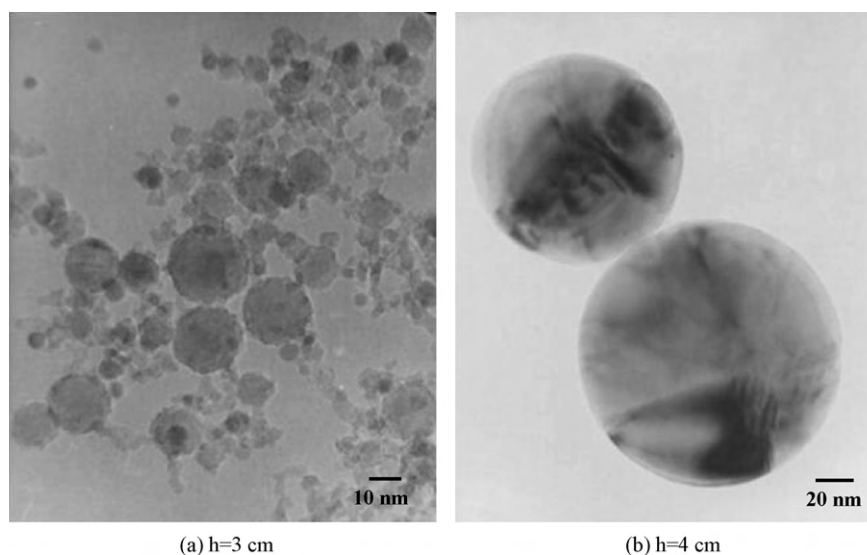


Fig. 12. TEM micrographs of synthesized titania nanoparticles collected at (a) $h = 3$ cm and (b) $h = 4$ cm ($\phi = 1.0$, TTIP = 0.32%, $O_2/N_2 = 40/60$).

Table 2

Measurements (BET, Z-average, TEM and XRD) for the titania powders synthesized at different molar ratios of O_2/N_2 .

$\phi = 1.0$ O_2/N_2	Pore volume (cm^3/g)	Pore size (nm)	BET SSA ^a (m^2/g)	D_p [BET] ^b (nm)	Z-Average ^c (nm)	Avg. D_p [TEM] ^d (nm)	Anatase%	Rutile%
Degussa P25	0.106	9.29	45.63	34.24	456.2	N/A	80	20
20/80	0.278	9.35	118.94	13.14	308.4	25	0	100
40/60	0.297	9.55	124.39	12.56	225.2	20	97.7	2.3

^a Particle SSA obtained from the BET instrument.

^b Average particle size calculated from BET method.

^c Mean particle diameter measured from Malvern Zetasizer Nano-ZS.

^d Average particle size calculated from TEM-counting.

of time at $\lambda = 465$ nm. The efficiency in the applied photocatalyst, with the nanosize anatase (20 nm, 97.7 wt.%) and high BET SSA ($124.39 m^2/g$), is better than that of Degussa P25. As an overall effect of surface area and appropriate crystallinity, the flame-synthesized titania showed higher photocatalytic activity than Degussa P25. The activity of titania decreased significantly due to the noticeable reduction of its specific surface area. It was found that the higher flame temperature led to better photocatalytic activity, but also a greater surface area.

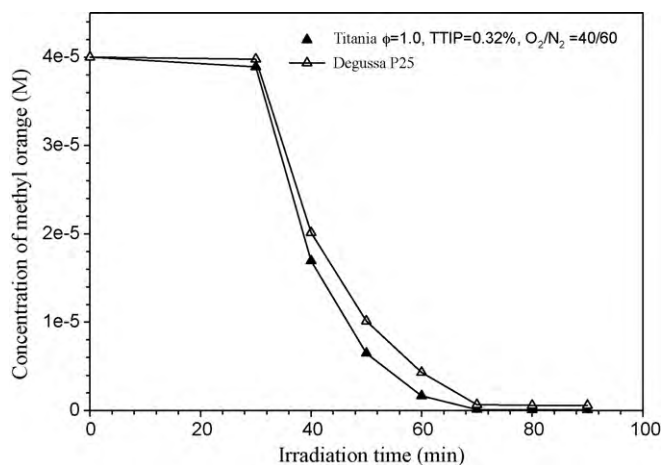


Fig. 13. Comparison on degradation curves of Degussa P25 and titania sample ($\phi = 1.0$, TTIP = 0.32%, $O_2/N_2 = 40/60$) with methyl orange.

4. Conclusions

TTIP is an appropriate titanium precursor for the as-synthesized titania nanoparticles in premixed flames. Increasing the TTIP molar fraction led to a more condensed and productive particle-laden region with a bright yellow flame brush. The smaller anatase titania nanoparticles formed at an optimum temperature of 1290 K. The titania crystal phase purity could be effectively controlled by the oxygen concentration in the premixed burner. A macroporous–mesoporous structure of titania was fabricated by the optimized condition of $\phi = 1.0$, TTIP = 0.32%, $O_2/N_2 = 40/60$, and $h = 3.0$ cm in premixed methane/air flames. Anatase (97.7 wt.%) nanoparticles with nanosize diameters (20 nm), small Z-averages (225.2 nm), high BET SSA values ($124.39 m^2/g$), large pore volumes ($0.297 cm^3/g$), and large pore sizes (9.55 nm) were found. The flame-synthesized titania nanoparticles ($\phi = 1.0$, TTIP = 0.32%, $O_2/N_2 = 40/60$) showed better photocatalytic activity regarding the removal of methyl orange. In truth, the optimum titania nanoparticles exceeded the conditions of the commercial Degussa P25 titania. A higher collecting height resulted in more primary nanoparticles in the early stage, so that more colliding chances between nanoparticles were allowed, which produced larger particles in the end. The growth of particles continued in the post-flame region, and nearly spherical particles of about 100–200 nm were formed at $h = 5$ cm.

Acknowledgment

This research was supported by the National Science Council of the R.O.C. under grant NSC 95-2221-E-002-337.

References

- [1] S.E. Pratsinis, Prog. Energy Combust. Sci. 24 (1998) 197–219.

- [2] A.H. Sun, P.J. Guo, Z.X. Li, Y. Li, P. Cui, *J. Alloys Compd.* 481 (2009) 605–609.
- [3] A. Beitollahi, A.H.H. Daie, L. Samie, M.M. Akbarnejad, *J. Alloys Compd.* 490 (2010) 311–317.
- [4] K.K. Akurati, A. Vital, U.E. Klotz, B. Bommer, T. Graule, M. Winterer, *Powder Technol.* 165 (2006) 73–82.
- [5] E. Setiawati, K. Kawano, *J. Alloys Compd.* 451 (2008) 293–296.
- [6] H. Chang, S.J. Kim, H.D. Jang, J.W. Choi, *Colloid Surf. A-Physicochem. Eng. Aspects* 313 (2008) 282–287.
- [7] C.A. Chen, Y.M. Chen, K.Y. Chen, J.K. Chi, Y.S. Huang, D.S. Tsai, *J. Alloys Compd.* 485 (2009) 524–528.
- [8] P. Periyat, D.E. McCormack, S.J. Hinder, S.C. Pillai, *J. Phys. Chem. C* 113 (2009) 3246–3253.
- [9] W.C. Chen, Y.T. Wang, C.J. Shih, *J. Alloys Compd.* 490 (2010) 576–581.
- [10] D.H. Kim, H.S. Hong, S.J. Kim, J.S. Song, K.S. Lee, *J. Alloys Compd.* 375 (2004) 259–264.
- [11] K.K. Akurati, A. Vital, G. Fortunato, R. Hany, F. Nueesch, T. Graule, *Solid State Sci.* 9 (2007) 247–257.
- [12] J.H. Jho, D.H. Kim, S.J. Kim, K.S. Lee, *J. Alloys Compd.* 459 (2008) 386–389.
- [13] E. Shafirovich, S.K. Teoh, A. Varma, *Combust. Flame* 152 (2008) 262–271.
- [14] Q.L. Zhou, C.Z. Li, F. Gu, H.L. Du, *J. Alloys Compd.* 463 (2008) 317–322.
- [15] S. Ameen, M.S. Akhtar, G.S. Kim, Y.S. Kim, O.B. Yang, H.S. Shin, *J. Alloys Compd.* 487 (2009) 382–386.
- [16] Y.J. Chen, M.C. Hsu, Y.C. Cai, *J. Alloys Compd.* 490 (2010) 493–498.
- [17] R.M. Trommer, A.K. Alves, C.P. Bergmann, *J. Alloys Compd.* 491 (2010) 296–300.
- [18] C.L. Yeh, S.H. Yeh, H.K. Ma, *Powder Technol.* 145 (2004) 1–9.
- [19] C.L. Yeh, E. Zhao, H.K. Ma, *Combust. Sci. Technol.* 173 (2001) 25–46.
- [20] R.A. Spurr, H. Myers, *Anal. Chem.* 29 (1957) 760–762.
- [21] S. Al-Qaradawi, S.R. Salman, *J. Photochem. Photobiol. A-Chem.* 148 (2002) 161–168.
- [22] M. Mikami, K. Yamaoto, O. Moriue, N. Kojima, *Proc. Combust. Inst.* 30 (2005) 2021–2028.
- [23] A.J. Rulison, P.F. Miquel, J.L. Katz, *J. Mater. Res.* 11 (12) (1996) 3083–3089.
- [24] S. Vemury, S.E. Pratsinis, *Appl. Phys. Lett.* 66 (24) (1995) 3275–3277.
- [25] S.E. Pratsinis, W. Zhu, S. Vemury, *Powder Technol.* 86 (1996) 87–93.
- [26] C.H. Hung, J.L. Katz, *J. Mater. Res.* 7 (1992) 1861–1869.